




Metasurface loaded twin-port microstrip antenna with circular polarization features for UHF RFID applications

Anand Vardhan Bhalla  and Agya Mishra

Department of Electronics & Communication Engineering, Jabalpur Engineering College, Jabalpur, India

Research Paper

Cite this article: Bhalla AV, Mishra A (2024) Metasurface loaded twin-port microstrip antenna with circular polarization features for UHF RFID applications. *International Journal of Microwave and Wireless Technologies*, 1–8. <https://doi.org/10.1017/S1759078724000989>

Received: 29 July 2024
Revised: 5 September 2024
Accepted: 15 September 2024

Keywords:

circular polarization; metamaterial absorber; MIMO antenna; RFID

Corresponding author:

Anand Vardhan Bhalla;
Email: anand.bhalla1983@gmail.com

Abstract

This communication designs and investigates a twin-port microstrip antenna loaded with a metasurface (MS). The proposed MS works in two ways: (i) artificial ground plane for radiator and (ii) as an ideal absorber of normal incoming waves at the same time. A stair shaped slot is loaded on rectangular patch for creating circularly polarized wave in between 835–894 MHz. Antenna port slots oriented in a mirror manner increase isolation by 25 dB. To act as a validation tool, the suggested antenna was built and its executions in individually operating modes evaluated by statistical and experimental analysis. It is shown that combining the patch and absorber results in a well-matched antenna in between 710–980 MHz with improved gain (more than 3.0 dBi). The proposed antenna design effectively used for UHF (Ultra High Frequency) radio-frequency identification (RFID) applications, which is due to its ability to mitigate multipath reflection issues and incorrect RFID reading.

Introduction

Low-profile antennas with comparatively tiny vertical cross sections have many uses in today's wireless communication systems, including emergency and military systems, consumer and industrial electronics, and more [1]. For both fixed and contemporary portable devices that combine consumer electronics with wireless communication and navigation, these kinds of antennas are in considerable demand. A well-known and extensively utilized technology that makes it possible to wirelessly identify physical items that are both stationary and moving is called radio-frequency identification, or RFID. It has practically limitless development potential. At the moment, UHF band, which runs from 0.902 to 0.928 GHz in the US and from 0.865 to 0.868 GHz in Europe, is the frequency that RFID technology uses the most frequently. This is because it provides an excellent balance between read spectrum, safety, power use, and invasive force characteristics in a free environment [2]. Strong electromagnetic (EM) interference is the main drawback of UHF RFID devices, and it gets worse at longer wavelengths. In particular, in an interior context where multiplex reflection interference strongly affects communication, inappropriate procedure would reduce the consistent communications [3, 4]. Because of this, the wireless communications industry developed an interest in reducing the multipath effect to provide precise and accurate identification [5–7]. There are different techniques utilized to reduce the multipath effect such as, metasurface (MS) absorber [8] and use of absorbing material such as ferrite or carbon [9]. These techniques are very expensive, large, and cumbersome [10–13]. Compactness can be achieved by using lumped components in the unit-cubicle [14]. The bandwidth part is limited for the same.

Particularly the ones that are sold, UHF RFID microstrip radiator are frequently large, bushy, and weighty [15–17]. Many air holes in the aerial layout [18–23], thick substrates [25–27], and high dielectric permittivity materials [24] were some of the strategies used in an attempt to potentially cover the whole RFID band (0.860–0.960 GHz) globally. Use of air holes increases the radiator frequency range and gain at the price of a massive shape, whereas high dielectric constant and thick substrates lead to a finer radiator frequency range in addition to increasing the excitation of surface waves inside the structure, which lowers directivity and radiation efficiency. Because the compactness of portable UHF RFID scanners puts a premium on compactness, low-profile antennas that strike a compromise between antenna properties are needed. It is commonly recognized that a quarter-wavelength separation between the radiating element and the ground plane is necessary to reduce the negative phase reversing impact of the metallic grounding on the radiator performance [28]. Because of the nature of the MS structure, in phase surface currents between the radiator and synthetic ground might shorten that distance if the antenna ground plane is used instead of the artificial ground. Moreover, patch antennas, which are negatively impacted by surface waves and have the capacity to halt their propagation, may readily include MSs

into their designs [29]. In this work, we refer to these MSs that are coupled with printed radiator as, MPAs (Microstrip Patch Antenna) for short. These have been studied before, mostly in the gigahertz range and the upper UHF band, either below the patch functioning as a synthetic ground plane [30–33] or at the patch level enclosing its circle [34, 35]. It was demonstrated that by enhancing antenna gain and bandwidth while reducing surface wave excitation, this combination might assist improve the front-to-back ratio. There is not much published research in the lower UHF frequency range [36–38]. A compact EBG and a two layer high-impedance surface metallic ground were positioned above 0.3 and 0.96 GHz dipole radiator in references [36] and [37], respectively. At 960 MHz, the hybrid-impedance surface (HIS) structure created in produced a gain increase of 4.2 dB. A circularly polarized grounded-patch antenna operating at two frequencies, 915 and 2450 MHz, was positioned in reference [38] above a HIS. The radiator has a gain of 3.1 dBi and a total thickness of 30 mm at 915 MHz.

Because of its enormous potential for creating low-profile, effective antennas, HIS structures were heavily used in the design of all previously described structures intended to enhance the functionality of conventional printed radiator employing MSs. No research has been done on the possibility of replacing the absorber in the MPA structure with an HIS. Together, they would offer two distinct roles that might improve antenna properties a bit beyond their current role as an absorber to lessen complex replication interfering in UHF RFID schemes. Thus, the primary objective of this communication is to verify and list the benefits and drawbacks of the latter assertion. In conjunction with full-wave simulations and tests, thorough assessments of electrical and physical modeling have been carried out in order to build the suggested double-functional MS patch antenna. This is how the rest of the paper is structured. The section titled “Geometry of the Complete MPA Structure” displays the geometric properties of the suggested MPA structure. The suggested MS absorber and coaxially fed patch antenna are carefully analyzed and designed in the “Analysis and design” section. The “Experimental results and discussion” section analyses the numerical and experimental data for each MPA capacity, confirming the validity of the proposed methodology. The “Conclusion” section contains the study’s final comments.

Antenna geometry and its analysis

The proposed dual-port MIMO (Multi Input Multi Output) antenna consists of dual-patch antenna (Fig. 1a) with a MS absorber structure (Fig. 1b) in place of the ground plane. It has the potential to be an RFID reader since it can function better in normal antenna mode and also serve as an absorber to decrease scattering. This may effectively lower the number of RFID systems that are incorrectly read in multipath environments. Figure 1c presents the shape and specific physical properties of the suggested antenna. The patch as well as MS absorber is printed on FR4 substrate ($\epsilon_r = 4.4$ and $\tan\delta = 0.02$) with a thickness of 1.6 mm [39].

Figure 2 illustrates the fluctuation in S-parameter for both single- and dual-port antennas in the absence of any MS absorber loading. The following scenarios are examined: (a) a single-port patch antenna with no stair slot loading; (b) a single-port patch antenna with stair slot loading; (c) a dual-port patch antenna with stair slot loading that is oriented the same way; and (d) a dual-port patch antenna with stair slot loading that is oriented in a mirror manner. Figure 2 yields several noteworthy observations.

The proposed antenna’s impedance matching is improved by the stair-shaped slot loading; the isolation level is improved by more than 25 dB due to the mirror orientation of the slot loading; the reflection coefficient features of the single- and dual-port antenna are nearly the same, which is necessary for a MIMO radiator; and (iv) the slot loading also shifts the resonant frequency to the lower side. A microstrip antenna’s slot loading supplies the increment in the patch’s actual current path. As a result, the antenna becomes compact and the resonant frequency drops [40].

The axial ratio fluctuation with and without a stair-shaped slot (with equal and unequal arm length) is depicted in Fig. 3. When a stair-shaped slot with uneven arm length is loaded, Fig. 3 shows that the axial ratio falls below 3 dB within the working region. The stair-shaped slot separates the E-field into two orthogonal components with roughly equal amplitude. The arm length variation produces the 90° phase shift between the orthogonal field components. It is a prerequisite for the creation of circular polarization (CP) waves [41].

Currently in development is a MS absorber unit cell that can reduce multipath reflection and imprecise RFID reading. A perfect MS absorber is one that balances external coupling and internal losses to prevent reradiation. By balancing the transmission and reflection power coefficients, this is accomplished. Since the structure’s backside is completely covered in copper, the transmission coefficient is 0, allowing the absorptivity (A) to be calculated by

$$A = 1 - |S_{11}|^2 \quad (1)$$

The inherent losses of resonant unit cells significantly restrict the overall achievable absorption. Effective dielectric losses with the right impedance matchings or the addition of internal losses through the use of resistive materials are two potential ways to further enhance the absorption properties. Changing the external coupling as an alternative to changing the internal losses is another way to regulate the absorption process. This statement can be understood by calculating the input impedance of MS near to resonance. It is given as follows [42]:

$$Z_{in}/Z_0 = \frac{1/Q_{ex}}{j2\delta + 1/Q_{in}} \quad (2)$$

where $\delta = (\omega - \omega_0)/\omega_0$ is the detuned degree, ω_0 is the angular resonant frequency, Q_{in} and Q_{ex} are the internal and external Q-factors, respectively, and Z_0 is the impedance in free space. It is easily deduced from (A) that a locus of Z_{in} forms a circle on the Smith chart with the diameter of $2Q_{in}/(Q_{in} + Q_{ex})$, assuming that Q_{in} and Q_{ex} are constant at the resonance. Since the impedance circle passes the origin (zero reflection) at the resonance, a complete absorption happens at the critical coupling of $Q_{in} = Q_{ex}$. Whereas Q_{ex} originates from the external coupling between the guided waves in the MS and the normal incident waves, Q_{in} originates from the conductor and dielectric losses in practical MSs [43, 44]. Reflection coefficient ($|S_{11}|$) in terms of internal losses ($\frac{1}{\tau_0}$) and external coupling ($\frac{1}{\tau_e}$) is given as follows [44]:

$$|S_{11}| = \frac{\left(\frac{1}{\tau_e}\right) - \left(\frac{1}{\tau_0}\right)}{\left(\frac{1}{\tau_e}\right) + \left(\frac{1}{\tau_0}\right)} \quad (3)$$

For $\left(\frac{1}{\tau_e}\right) = \left(\frac{1}{\tau_0}\right)$, i.e. the resonant frequency, there is no reflection, meeting the critical coupling requirement. It should be

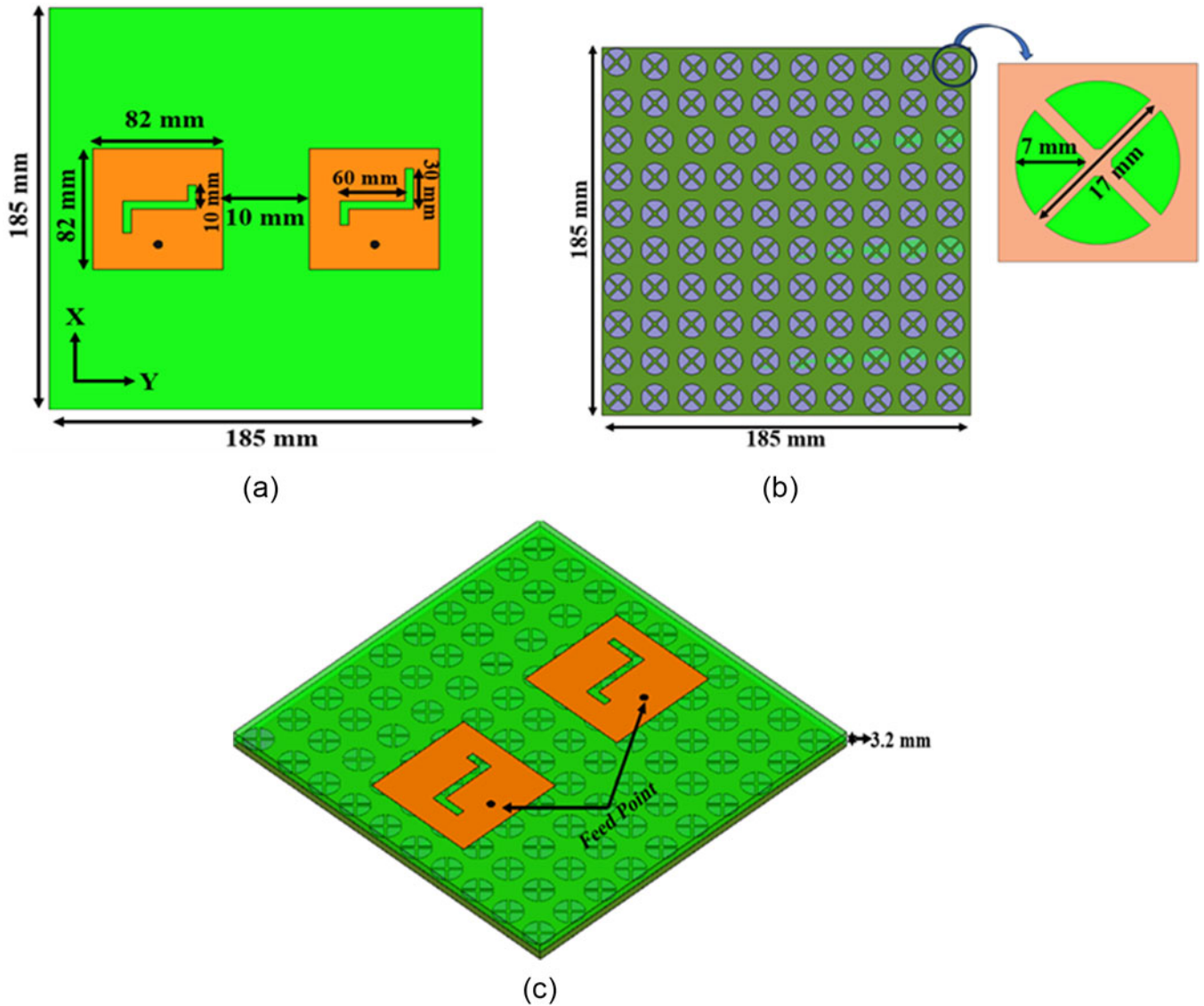


Figure 1. Geometrical layout of two-port MIMO antenna (a) front view of stair shaped slot loaded patch; (b) front view of metasurface absorber; (c) 3D layout of proposed antenna.

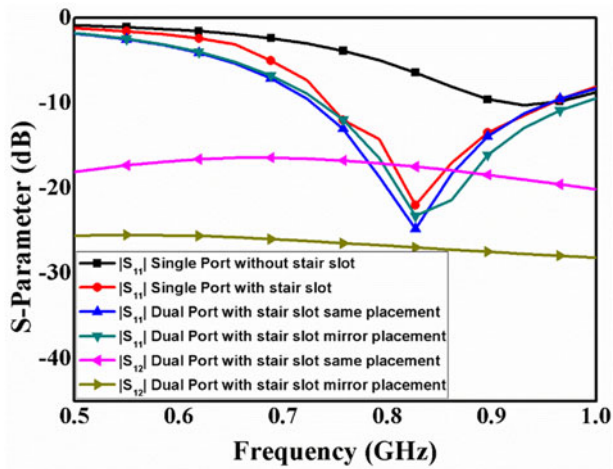


Figure 2. S-parameter variation with single- and dual-port antenna without any MS absorber.

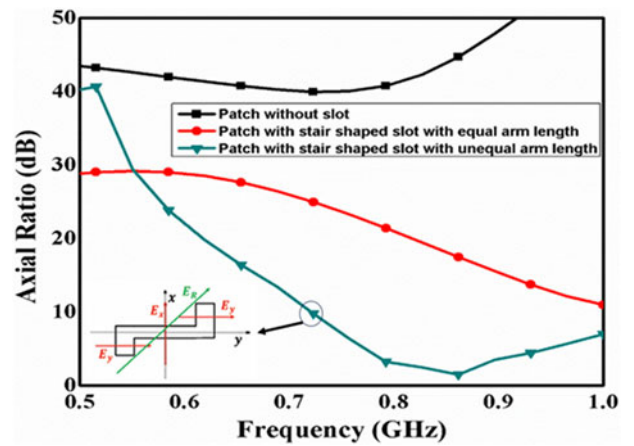


Figure 3. Axial ratio variation with and without loading of stair-shaped slot.

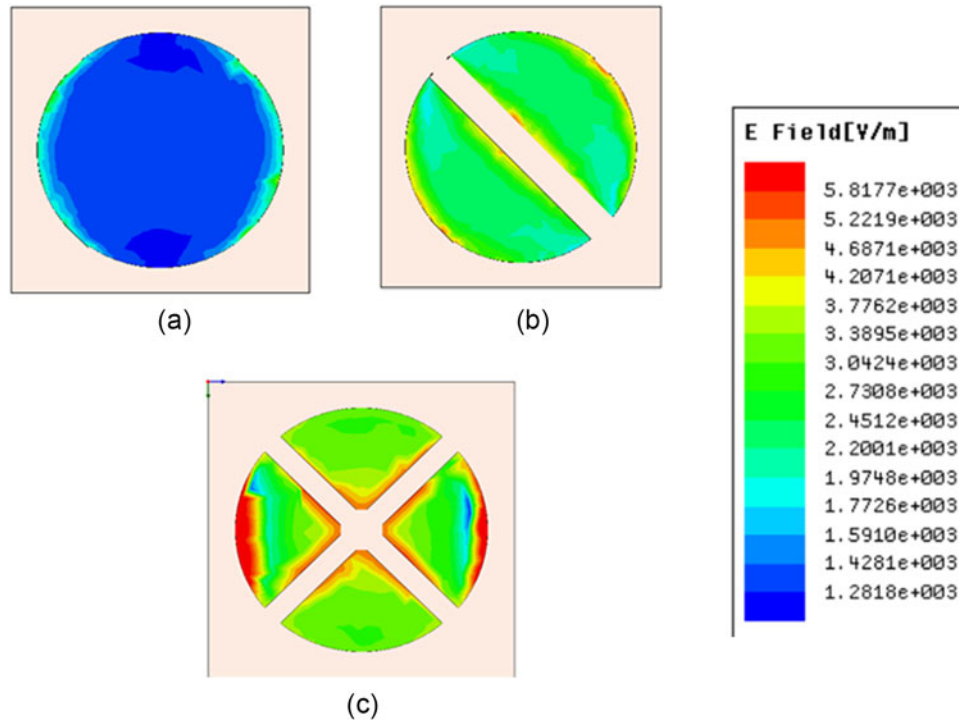


Figure 4. E-field distribution at the top surface of the unit-cell design stages for an 868 MHz normal incident plane wave (a) circular patch without any slit (b) circular patch with one diagonal slit (c) circular patch with two diagonal slits.

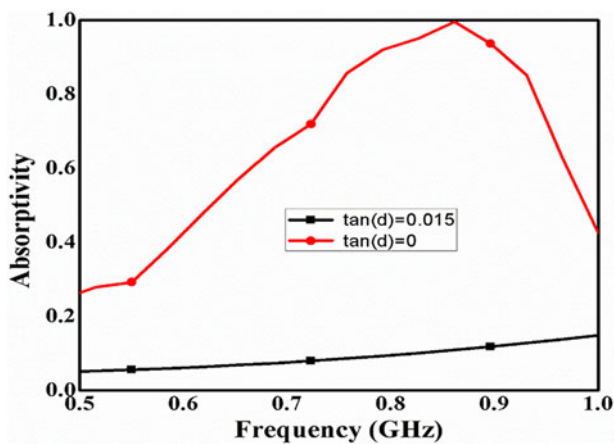


Figure 5. Absorptivity variation with change in loss tangent value.

mentioned that the resonator is said to be over coupled when $\left(\frac{1}{\tau_c}\right) > \left(\frac{1}{\tau_0}\right)$, and under coupled when $\left(\frac{1}{\tau_c}\right) < \left(\frac{1}{\tau_0}\right)$. The rate of power escape from the resonant structure (MS absorber at resonance) is higher in the overcoupled area than the rate of internal dissipation. When considering the undercoupled scenario, internal losses surpass power leakage from the structure in terms of quantity.

The current study aims to meet the critical coupling requirement irrespective of the unit-cell size by optimizing that method in the megahertz range. We want to show how a straightforward unit cell with good reflection properties may be tuned to be the ideal absorber for normal incident waves on a substrate of the same dimensions and kind. Perfect absorption was attained by altering

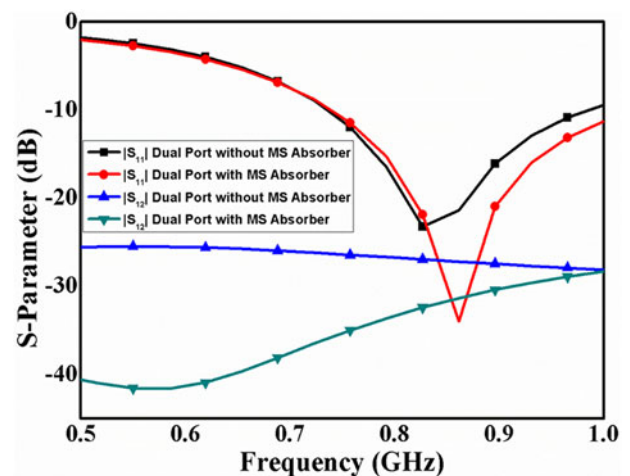


Figure 6. S-parameter variation of dual-port antenna in presence/absence of MS absorber.

the external connection, which was accomplished by appropriately slicing diagonal slits on the metal circular patch. The patch underwent a first diagonal incision to lengthen the current channel and lower the resonance frequency. It also caused the region to become undercoupled as opposed to overcoupled. To symmetrize the E distribution locally with regard to the incident wave polarization – which is concentrated along the y-axis at the unit cell edges – a second slot was incorporated into the construction. This situation is explained in detail in Fig. 4, which shows the E-field distribution in three different scenarios: (a) an unslotted patch; (b) a circular patch with a single diagonal slit; and (c) a circular patch with two diagonal slits.

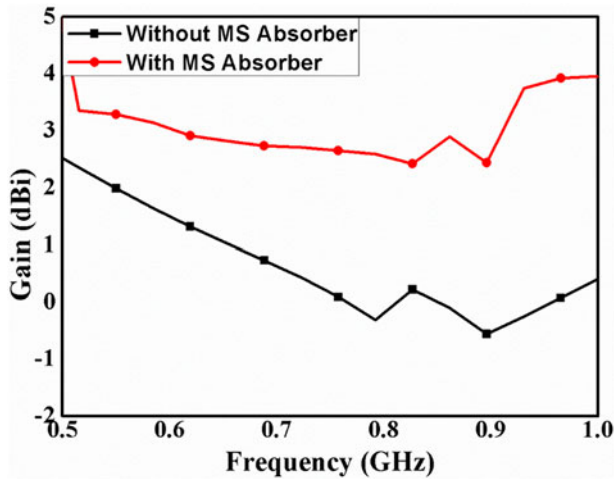


Figure 7. Gain variation of dual-port antenna in presence/absence of MS absorber.

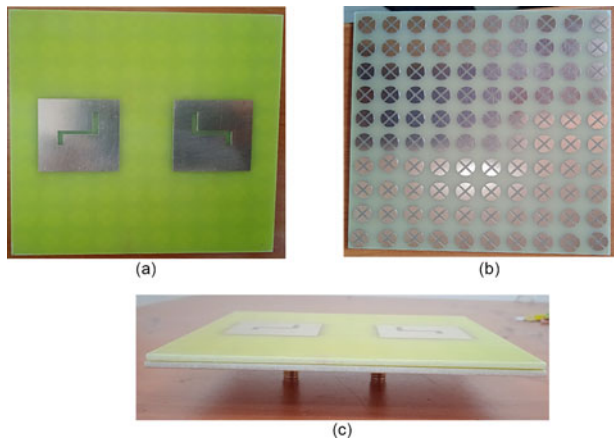


Figure 8. Pictures of fabricated prototype of designed radiator (a) top view (b) MS absorber (b) 3D view of designed radiator.

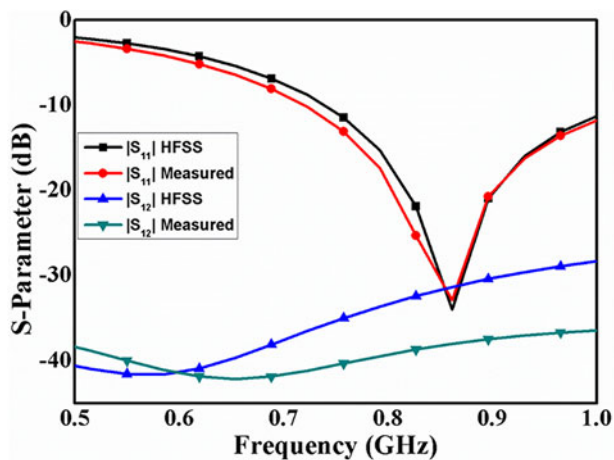


Figure 9. Measured/simulated S-parameter of proposed antenna design.

It is crucial to keep in mind that the Poynting theorem links the imaginary component of permeability and permittivity to the real part of the mean power as time passes. Therefore, one of the most important factors in achieving 100% absorption is the dielectric

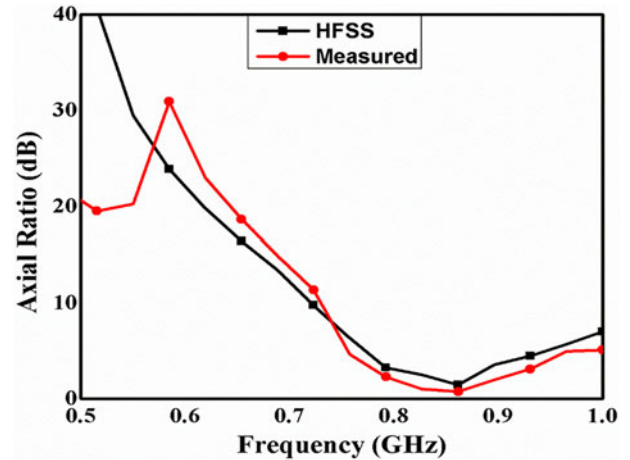


Figure 10. Measured/simulated axial ratio variation of proposed antenna.

$\tan\delta$. The Poynting theorem states that the real components of the meta-surface absorber (MSA) permittivity (ϵ) and permeability (μ) are engaged with the resonance of the MSA along the incident wave's path [45, 46]. This explains why the stored power in the near-field of MEH switches between reactive magnetic and electric fields with each time-harmonic field cycle. While these components are necessary to generate the MSA resonance, they may be disregarded in order to compute the actual portion of average power [45, 47]. On the other hand, at the resonance frequency of MEH, the imaginary components of ϵ and μ operate as power consumption, and a real resistance may mimic the EM response [45]. It should be noted that an equal quantity of magnetic and electric energy may be carried by an EM wave traveling in free space. This is because, prior to exchanging their energy with the energy of the meta-atom, these traveling waves are in a balanced condition at the free-space medium [47]. In fact, this balance is maintainable, and in a perfect MS with no reflections, the majority of the incoming wave's actual average power is used at the loads. In this instance, the latter was accomplished by managing exterior bonding on a low-loss unit-cell material that had a $\tan\delta$ of just 0.0015.

To demonstrate how the loss tangent influences absorbent properties, Fig. 5 simulates the absorption variation of the suggested unit cell with change in $\tan\delta$. At unity magnitude, the behavior of the lossless unit cell is similar to that of a typical HIS reflector, and at $\tan\delta = 0.0015$, nearly total absorption was achieved. Figure 6 displays the fluctuation of the S-parameter with and without the MS absorber after the unit cell has been converted into an array and put on the bottom part of the radiator. Figure 6 presents that the properties of the reflection coefficient are about the same in both scenarios. In other words, the intrinsic characteristics of the antenna remain unaffected by the suggested MS absorber's loading. In all scenarios, there is about the same isolation among the ports. The gain fluctuation with and without an MS absorber is exposed in Fig. 7. It can be perceived from Fig. 7 that the inclusion of an MS absorber increases the gain value to 2–3 dBi. Notably, $|S_{11}|$ can approach 0 over a substantial percentage of the proposed absorber, in contrast to high-impedance surface, where the $|S_{11}|$ magnitude at the resonant frequency is 1. Thus, the absorber in combination with the normal patch antenna not only yields a noticeable gain boost but may also help enhance the fading situation of RFID schemes by decreasing the severe complex replication interference and crash difficulties.

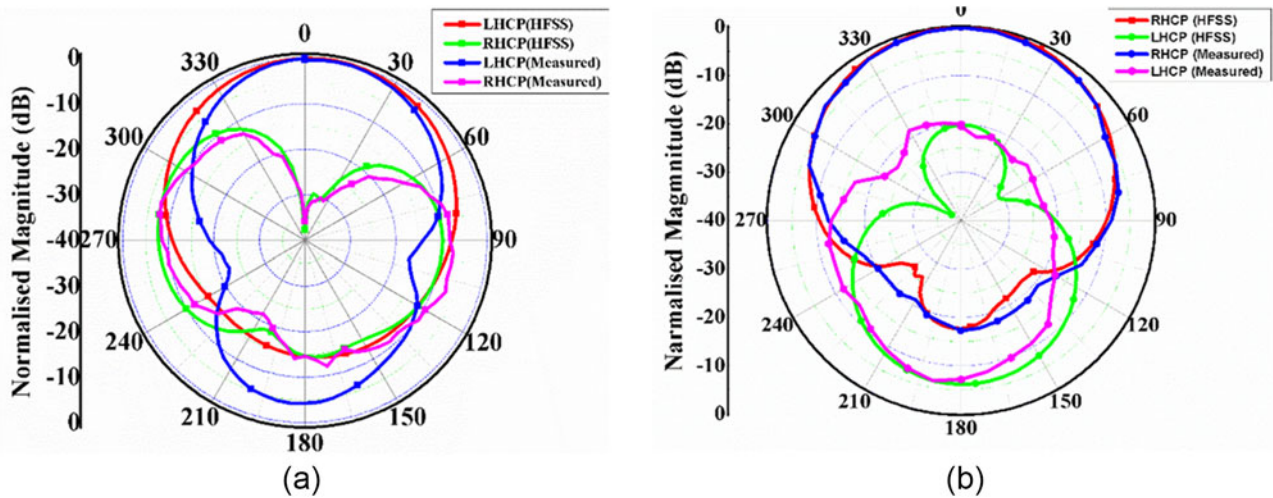


Figure 11. Measured/simulated RHCP and LHCP of proposed radiator at 0.86 GHz (a) port-1 (b) port-2.

Experimental verification and discussion

This stage involves testing the suggested antenna prototype to validate the optimum outcomes. Figure 8 shows pictures of the built prototype of the proposed antenna. It is made on FR-4 dielectric, which has a dielectric constant of 4.4. The two-port radiator is positioned beneath the MS absorber. The suggested antenna's measured and simulated S-parameter is displayed in Fig. 9. It is tested with an E5071C vector network analyzer that is based on Keysight. It is verified by Fig. 9 that the simulated and observed S-parameters have a strong correlation. The suggested antenna has an isolation level of more than 25 dB and operates efficiently in the frequency range of 710–980 MHz.

The suggested antenna's observed and predicted axial ratio fluctuation is displayed in Fig. 10. Dual linear pattern measuring is used to measure it [48]. It is evident from Fig. 10 that the simulated and observed axial ratios accord rather well. The CP waves in the range of 835–894 MHz are supported by the suggested radiator. The simulated and observed LHCP (Left handed Circular Polarization) and RHCP (Right handed Circular Polarization) far-field pattern at 0.86 GHz in the XZ plane is displayed in Fig. 11. It can be perceived from Fig. 11 shows that LHCP waves with port-1 and RHCP waves with port-2 are supported by the suggested radiator. This indicates that the polarization diversity idea is supported by the suggested antenna. The generated and measured patterns correspond rather well. The suggested antenna design's gain change in the broadside direction is shown in Fig. 12. Two antenna approach is used to measure it [48]. It is verified from Fig. 12 that the working band's maximum antenna gain is about 3.0 dBi.

The diversity parameters, or the diversity gain (DG) and envelope correlation coefficient (ECC) fluctuation for the planned multiport radiator, are shown in Fig. 13. The similarity content between ports 1 and 2 is expressed by ECC. It should be low (less than 0.2) for effective radiator design [49]. The gain of a multiport radiator in a fading environment is expressed as DG. Its value for an efficient antenna is around 10.0 dB [49]. It is verified from Fig. 13 that, within the operational band, the value of DG is around 10.0 dB and the value of ECC is less than 0.1. Table 1 is used to evaluate the intended radiator's performance with other current antennas in terms of gain, axial ratio bandwidth, and antenna size. From Table 1, it is clearly observed that the proposed antenna design first time proposed a two-port MIMO along with

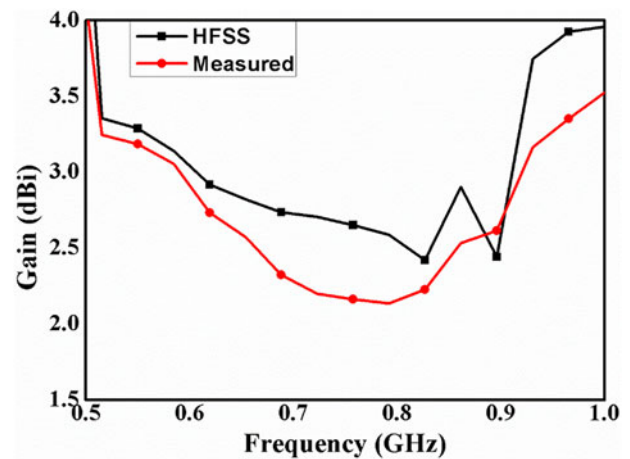


Figure 12. Measured/simulated gain variation of proposed antenna toward broadside direction.

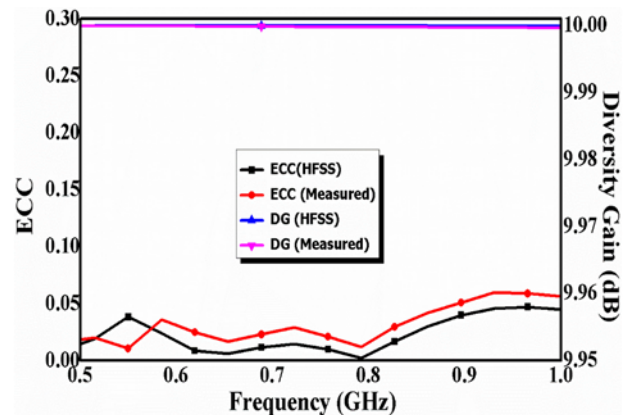


Figure 13. Measured/simulated ECC and DG variation of proposed antenna.

CP characteristics and loaded with metamaterial absorber for UHF RFID application. The proposed antenna is compact in size as well as provides the good gain value as compared to other radiation structure.

Table 1. Performance assessment of proposed dual-port printed antenna with other existing antenna on the basis of absolute/axial ratio bandwidth, gain and antenna size

Antenna design	No. of ports	Impedance bandwidth (MHz)	Axial ratio bandwidth (MHz)	Gain (dBi)	Antenna size
[18]	01	120.0	NA	2.3	250 × 250 × 35
[19]	01	250.0	NA	2.5	200 × 200 × 19
[20]	01	123.0	NA	2.6	250 × 250 × 36
[21]	01	250.0	NA	2.8	200 × 200 × 60
[22]	01	118.0	NA	2.6	460 × 460 × 47
[23]	01	76.0	NA	2.7	200 × 200 × 12
Proposed antenna	02	270.0	60.0	3.0	185 × 185 × 3.23

Conclusion

For RFID uses in the 0.868 GHz band, a two-port MS microstrip radiator with dual functionality – that is, antenna and absorbent modes – was presented. The antenna architecture consists of two coaxially fed patch antennas filled with stair-shaped slots and a MS absorber performing as a synthetic ground. It seemed interesting to incorporate a MS absorber into the antenna construction to create a reader antenna that can reduce fading replication and inappropriate RFID reading, which is important for the uses that are being considered. Within the operational band, which is 835–894 MHz, stair-shaped slot loading generates the CP waves. The slot's mirror image improves isolation by more than 30 dB and offers polarization variety. The suggested antenna has a gain of 3.0 dBi, which is significantly larger than that of a traditional patch radiator. These results demonstrate that the proposed twin-port radiator can compete with existing RFID readers, indicating that it might be a good choice for future mobile or fixed RFID applications.

Funding statement. This research received no specific grant from any funding agency, commercial or not-for-profit sectors.

Competing interests. The authors report no conflict of interest.

References

- Convergence system limited Inc., CSL CS772 linear polarized RFID far field antenna. <https://www.convergence.com.hk/pro-duct/cs772/>. (accessed 11 Dec 2020).
- Engels DW and Sarma SE The reader collision problem. In *IEEE International Conference Systems, Man Cybernetics, Yasmine Hammamet, Tunisia*, vol. 3, 92–97 (2002).
- Costa F, Genovesi S, Monorchio A and Manara G (2014), Low-cost metamaterial absorbers for sub-GHz wireless systems. *IEEE Antennas and Wireless Propagation Letters* **13**, 27–30. 10.1109/LAWP.2013.2294791
- Veneri F, Costanzo S and Di Massa G (2018), Fractal-shaped metamaterial absorbers for multireflections mitigation in the UHF band. *IEEE Antennas and Wireless Propagation Letters* **17**, 255–258. 10.1109/LAWP.2017.2783943
- Mohamed-Hicho NM, Antonino-Daviu E, Cabedo-Fabrés M and Ferrando-Bataller M (2015), A novel low-profile high-gain UHF antenna using high-impedance surfaces. *IEEE Antennas and Wireless Propagation Letters* **14**, 1014–1017. 10.1109/LAWP.2015.2389274
- Collin RE (1992), *Foundations for Microwave Engineering*. New York, NY, USA: McGraw-Hill.
- Costa F, Genovesi S, Monorchio A and Manara G Ultra-thin absorbers for ultra-high frequency RFID systems. In: *IEEE Antennas Propagation Society International Symposium (APS/URSI), Orlando, FL*, 1500–1501 (2013).
- Haus HA (1984), *Waves and Fields in Optoelectronics*. Englewood Cliffs: Prentice-Hall Inc..
- Times-7 Inc., A4030L SlimLine linear polarization RFID reader Antenna. <https://www.times-7.com/a4030l-linear-polarised-uhfantenna.html>. (accessed 11 Dec 2020).
- Sarkar S and Gupta B (2020), A dual-band circularly polarized antenna with a dual-band AMC reflector for RFID readers. *IEEE Antennas and Wireless Propagation Letters* **19**, 796–800. 10.1109/LAWP.2020.2980325
- Wang N, Dong X., Zhou W., He C., Jiang W. and Hu S., (2016), Low-frequency metamaterial absorber with small-size unit cell based on corrugated surface. *AIP Advances* **6**, 025205. 10.1063/1.4941933
- Nestoros M, Christou MA and Polycarpou AC (2017), Design of wide-band, circularly polarized patch antennas for RFID applications in the FCC/ETSI UHF bands. *Progress In Electromagnetics Research C* **78**, 115–127. 10.2528/PIERC17071801
- Hung Tien Nguyen SN and Shafai L, “Microstrip patch miniaturization by slots loading” 2005 IEEE Antennas and Propagation Society International Symposium, Washington, DC, USA, 03-08 July 2005
- Best SR and Hanna DL (2008), Design of a broadband dipole in close proximity to an EBG ground plane. *IEEE Antennas and Propagation Magazine* **50**, 52–64. 10.1109/MAP.2008.4768923
- Kovitz JM and Rahmat-Samii Y (2014), Using thick substrates and capacitive probe compensation to enhance the bandwidth of traditional CP patch antennas. *IEEE Transactions on Antennas and Propagation* **62**, 4970–4979. 10.1109/TAP.2014.2343239
- Wang Z and Dong Y (2020), Miniaturized RFID reader antennas based on CRLH negative order resonance. *IEEE Transactions on Antennas and Propagation* **68**, 683–696. 10.1109/TAP.2019.2940500
- Waltonchain UHF RFID ceramic antenna IOT-CT03. <https://www.waltonchain.org/en/sys/348.html>. (accessed 11 Dec 2020).
- Sim C, Hsu Y and Yang G (2015), Slits loaded circularly polarized universal UHF RFID reader antenna. *IEEE Antennas and Wireless Propagation Letters* **14**, 827–830. 10.1109/LAWP.2014.2382557
- Take R, Okano Y and Noda K Development of the ultrathin microwave absorber composed of soft material. In: *IEEE Asia-Pacific Microwave Conference Singapore*, 174–176 (2019)
- Elsheakh DMN, Hala HA, and Abdallah EA (2012), *Antenna Designs with Electromagnetic Band Gap Structures*. London: IntechOpen.
- Glybovski SB, Tretyakov SA, Belov PA, Kivshar YS and Simovski CR (2016), Metasurfaces: From microwaves to visible. *Phys. Rep* **634**, 1–72.
- Baracco J, Salghetti-Drioli L and de Maagt P (2008), AMC low profile wideband reference antenna for GPS and GALILEO systems. *IEEE Transactions on Antennas and Propagation* **56**, 2540–2547. 10.1109/TAP.2008.927547
- Zuo W, Yang Y, He X, Zhan D and Zhang Q (2017), A miniaturized metamaterial absorber for ultrahigh-frequency RFID system. *IEEE Antennas and Wireless Propagation Letters* **16**, 329–332. 10.1109/LAWP.2016.2574885
- Amano M, and Kotsuka Y (2003), A method of effective use of ferrite for microwave absorber. *IEEE Transactions on Microwave Theory and Techniques* **51**, 238–245. 10.1109/TMTT.2002.806912
- Nasimuddin N, Qing X and Chen ZN (2013), A wideband circularly polarized stacked slotted microstrip patch antenna. *IEEE Antennas and Propagation Magazine* **55**, 84–99. 10.1109/MAP.2013.6781708
- Okano Y, Ogino S and Ishikawa K (2012), Development of optically transparent ultrathin microwave absorber for ultrahigh-frequency RF identification system. *IEEE Transactions on Microwave Theory and Techniques* **60**, 2456–2464. 10.1109/TMTT.2012.2202680
- Boutayeb H and Denidni TA (2007), Gain enhancement of a microstrip patch antenna using a cylindrical electromagnetic crystal substrate. *IEEE Transactions on Antennas and Propagation* **55**, 3140–3145. 10.1109/TAP.2007.908818

28. **Veneri F, Costanzo S and Borgia A** (2019), A dual-band compact metamaterial absorber with fractal geometry. *Electronics* **8**, 87. 10.3390/electronics8080879
29. **Agarwal K, Nasimuddin N and Alphones A** (2012), Compact asymmetric-slotted-slit patch based circularly-polarized antenna with reactive impedance surface substrate. *Microwave and Optical Technology Letters* **54**, 2505–2510. 10.1002/mop.27147
30. **Stutzman WL, and Thiele GA** (2013), 'Antenna Theory and Design'. New York: A, John Wiley & Sons, INC., Publication.
31. **Yuan W and Cheng Y** (2014), Low-frequency and broadband metamaterial absorber based on lumped elements: Design, characterization and experiment. *Appl. Phys. A* **117**, 1915–1921. 10.1007/s00339-014-8637-3
32. **Wang Z, Fang S, Fu S and Jia S** (2011), Single-fed broadband circularly polarized stacked patch antenna with horizontally meandered strip for universal UHF RFID applications. *IEEE Transactions on Microwave Theory and Techniques* **59**, 1066–1073. 10.1109/TMTT.2011.2114010
33. MTI wireless edge Inc., MT-263003/N linear polarization RFID panel antenna. <https://www.mtiwe.com/?CategoryID=219&ArticleID=71>. (accessed 11 Dec 2020).
34. **Gupta G, Singh BP, Bal A, Kedia D and Harish AR** (2014), Orientation detection using passive UHF RFID technology [Education Column]. *IEEE Antennas and Propagation Magazine* **56**, 221–237. 10.1109/MAP.2014.7011063
35. **Kato Y, Morita S, Shiomi H and Sanada A** (2020), Ultrathin perfect absorbers for normal incident waves using dirac cone metasurfaces with critical external coupling. *IEEE Microwave and Wireless Components Letters* **30**, 383–386. 10.1109/LMWC.2020.2979708
36. **Ahson AS and Ilyas M** (2008), *RFID Handbook: Applications, Technology, Security and Privacy*. Boca Raton: CRC Press.
37. **Sharawi MS** (2014), Printed MIMO Antenna Engineering. Norwood, MA, USA: Artech House.
38. **Ghaneizadeh A, Mafinezhad K and Joodaki M** (2019), Design and fabrication of a 2D-isotropic flexible ultra-thin metasurface for ambient electromagnetic energy harvesting. *AIP Advances* **9**, 025304. 10.1063/1.5083876
39. **Ghaneizadeh A, Mafinezhad K and Joodaki M** (2020), An extremely ultrathin flexible Huygens's transformer. *AIP Advances* **10**, 105201. 10.1063/5.0016373
40. **Chen ZN, Qing X and Chung HL** (2009), A universal UHF RFID reader antenna. *IEEE Transactions on Microwave Theory and Techniques* **57**, 1275–1282. 10.1109/TMTT.2009.2017290
41. **Nasimuddin N, Chen ZN and Qing X** (2010), Asymmetric-circular shaped slotted microstrip antennas for circular polarization and RFID applications. *IEEE Transactions on Antennas and Propagation* **58**, 3821–3828. 10.1109/TAP.2010.2078476
42. **Balanis CA** (2005), "Antenna Theory: Analysis and Design" A. New York: John Wiley & Sons, INC., Publication.
43. **Mumby S and Yuan J** (1989), Dielectric properties of FR-4 laminates as a function of thickness and the electrical frequency of the measurement. *Journal of Electronic Materials* **18**, 287–292. 10.1007/BF02657420
44. **Zhao R, Zhu Z, Dong G, Lv T, Li Y, Guan C, Shi J and Zhang H** (2019), High efficiency Huygens' metasurface for terahertz wave manipulation. *Optics Letters* **44**, 3482–3485. 10.1364/OL.44.003482
45. **Bao XL, Ruvio G and Ammann MJ** (2009), Directional dual-band slot antenna with dual-bandgap high-impedance-surface reflector. *Progress In Electromagnetics Research C* **9**, 1–11. 10.2528/PIERC09051505
46. **Augustin G, Rao Q, and Denidni TA** (2016), Low-Profile Antennas. *Handbook of Antenna Technologies*. Springer: Berlin, pp. 145–149.
47. **Baggen R et al.** (2008), Low profile GALILEO antenna using EBG technology. *IEEE Transactions on Antennas and Propagation* **56**, 667–674. 10.1109/TAP.2008.916927
48. **Nakamura T and Fukusako T** (2011), Broadband design of circularly polarized microstrip patch antenna using artificial ground structure with rectangular unit cells. *IEEE Transactions on Antennas and Propagation* **59**, 2103–2110. 10.1109/TAP.2011.2143656
49. **Ghaneizadeh A, Joodaki M, Börcsök J, Golmakani A and Mafinezhad K** (2020), Analysis, design, and implementation of a new extremely ultrathin 2-D-isotropic flexible energy harvester using symmetric patch FSS. *IEEE Transactions on Microwave Theory and Techniques* **68**, 2108–2115. 10.1109/TMTT.2020.2982386



Anand Vardhan Bhalla is pursuing PhD under the supervision of Prof. Agya Mishra at the Department of Electronics and Telecommunication Engineering, Jabalpur Engineering College, Jabalpur, Madhya Pradesh, India affiliated to Rajiv Gandhi Proudhyogiki Vishwavidyalaya, Bhopal, Madhya Pradesh, India. He earned his M.Tech in Digital Communication from Gyan Ganga College of Technology, Jabalpur,

Madhya Pradesh, India and his B.E. in Electronics and Communication Engineering from Indira Gandhi Government Engineering College Sagar, Madhya Pradesh, India, in 2012 and 2005, respectively. With over a decade of experience in academia, he has served as an Assistant Professor at Engineering Institutions across India. His research career spans more than 10 years, during which he has published over 35 research papers in journals of repute. He also holds two patents, reflecting his contributions to his field. His work has more than 500 citations. His research interests are broad and include Digital Communication, Artificial Intelligence, Machine Learning, IoT, and Signal Processing.



Agya Mishra is presently Head of Department of Artificial Intelligence and Data Science and Professor in Department of Electronics and Telecommunication Engineering, Jabalpur Engineering College, Jabalpur, Madhya Pradesh, India affiliated to Rajiv Gandhi Proudhyogiki Vishwavidyalaya, Bhopal, Madhya Pradesh, India. Her qualification includes PhD and M.Tech from Maulana Azad National Institute of Technology, Bhopal, Madhya Pradesh, India and has done

B.E. from Government Engineering College, Ujjain, Madhya Pradesh, India. She has more than 100 publications globally, having over 400 citations. She is an AI system designer, AI consultant, Academician, PhD guide and Journal reviewer.